1. Introduction

There is a significant demand for lightweight materials in the aerospace and automotive industries because such materials can substantially improve fuel efficiency and contribute to the reduction of CO_2 emissions. Carbon fiber–reinforced plastic (CFRP) is a representative lightweight material that can replace traditional metal materials. Compared to metals, CFRP requires considerable molding expenses for structural applications, which is a real challenge for their practical application.

Recent trends show a global shift from the use of traditional thermoset CFRP to thermally responsive carbon fiber–reinforced thermoplastics (CFRTPs). CFRTPs have already been used in the rudder and elevator of business jets, the front edge of airplane wings, and the horizontal tail of helicopters[1] . Although the molding technology for CFRTP has significantly advanced in recent years, joining required for assembly after molding remains problematic. Adhesive bonding, mechanical fastening, and thermal fusion or welding are possible bonding methods for CFRTP. The chemical stability of thermoplastic resins, which typically makes them difficult to bond, can complicate the use of adhesive joining methods. In addition, joining methods that rely on the chemical reaction of adhesives can limit the joining speed.

Mechanical fastening approaches are also problematic in terms of joining speed because of the need for hole drilling; furthermore, the weight of rivets and bolts hinders the overall weight reduction. Thermal welding is a joining technique in which materials are heated under pressure, causing the interface to melt and solidify. Owing to higher joining speed compared to alternative methods, welding is primarily used as a joining technique for thermoplastics[2,3]. Ultrasonic welding is a type of thermal welding where ultrasonic vibrations are applied to the adherend resulting in frictional and viscoelastic heating of the joining surface.

This technique is one of the most material- and energy-efficient welding techniques available[4]. Ultrasonic welding is susceptible to issues with temperature control because of swift thermal escalation, which can lead to a reduction in strength because of resin thermal decomposition and excessive resin/fiber flow.

Placing an energy director (ED) at the interface can suppress the thermal degradation of the resin and the flow of fibers in the adherend. However, the application of an ED increases the number of processes, decreasing productivity[5]. Several previous studies have investigated welding conditions, adherend materials, and the effect and shape of EDs. The welding mechanism has been attempted to be elucidated

based on experimental results, such as power curves (time history of oscillator power), temperature history of the welding interface, and fracture surface shape[6-12]. However, temperature evaluation using thermocouples has its problems. The thermocouple itself may influence heat generation, and because it measures the temperature in a single point, the information it provides is not worth the effort required for installation.

To predict the temperature in areas where measurement is difficult during experiments, researchers have simulated heat generation and heat transfer near the interface using the finite element method[13, 14]. In the ultrasonic welding process, a time scale difference exists between the welding time (approximately 1 s) and the vibration cycle (approximately 10^5 s). Therefore, efforts must be made to reduce computational costs. In previous studies utilizing the finite element method, the sonotrode and anvil were often omitted from the model to expedite the analysis time.

Koyanagi et al. performed a finite element analysis using a two-dimensional ultrasonic welding model for flat ED and triangular ED shapes. In this study, to reduce the analysis time, parameters such as frequency, density, specific heat, and thermal capacity, which are different from those in the actual experiment, were used for the analysis[15]. As of now, temperature distribution during welding has not been sufficiently studied, whereas temperature distribution is crucial for comparing analytical results. This makes it difficult to validate the accuracy of the analytical models developed. Hence, techniques for experimentally measuring and evaluating the temperature distribution must be developed to enable a comparison and validation of the analytical models.

In the present study, we measured and analyzed the temperature distribution during ultrasonic welding of carbon fiber–reinforced polypropylene (CF/PP) plates. The temperature distribution of the side of the overlapping area of the lap joint was measured using a thermographic camera. The temperature distribution obtained was analyzed using the half-width method to investigate the temporal change in the temperature gradient in the thickness direction of the adherend, centered on the welding interface.

2. Measurement equipment and methods

2.1. Materials and specimen geometry

CF/PP prepreg sheets (TAFNEX, Mitsui Chemicals) with a lamination configuration of $(0/90)_{8S}$ were used in ultrasonic welding experiments. The prepreg sheets were consolidated in a hot press at a pressure of 2 MPa, temperature of 180 °C, and pressurization time of 3 min. The specimen geometry

conformed to the ISO 4587 standards. The adherend had a length of 100 mm, width of 25 mm, and thickness of 2.4 mm. Additionally, the overlap length was 12.5 mm. For specimen fabrication, a water jet cutting machine was used. In the present study, welding tests were performed without the ED.

2.2. Ultrasonic welding and the temperature measurement method

An ultrasonic welding machine (SONOPET DΣ2210SL/DΣ80SL, Seidensha Electronics Industry) was utilized to conduct welding experiments. An aluminum jig was used to fix the specimen during welding, as shown in Fig. 1. The jig was equipped with two linear bushes that allow for vertical sliding to prevent misalignment with the sonotrode, upper adherend, and lower adherend. The sonotrode made of aluminum featured a square tip measuring 30 mm on each side. The ultrasonic welding machine was operated at an oscillator frequency of 19.15 kHz; uniform welding was performed with a pressure of 312.5 N (1 MPa added to the lapping surface). Nine sets of welding conditions, each with three sonotrode amplitudes (36, 54, and 72 μm) and three welding times, were used in the welding tests. In the present study, temperature measurement experiments using a thermographic camera were performed under welding conditions that produce the maximum strength. The temperature distribution of the specimen during welding was analyzed from a side of the overlapping area using an infrared-thermography camera (R300SR, InfReC). The area of the adherend captured by the thermography camera is exhibited in Fig. 2. The temperature was measured from the side of the overlapping area. The amount of heat generated at the heat-generating point and the heat transfer in the thickness direction were determined based on the temperature distribution in the Y direction from the sonotrode tip center line (Fig. 2). The half-width method was used for the maximum temperature and the temperature distribution centered on the welding interface.

2.3. Lap shear strength tests

Lap shear tests were conducted using a mechanical universal testing machine (AG-100kN Xplus, Shimadzu Corporation) equipped with a hydraulic chuck. The tests were performed at a crosshead speed of 2 mm/min. The fracture surfaces of the weld specimens after the lap shear test were observed via digital microscopy (VHX-6000, Keyence).

3. Experimental results and discussions

3.1. Lap shear test

The results of the adhesive shear test at each amplitude are presented in Table 1 and the fracture surface after the test in Fig. 3. At high amplitudes, a short welding time is sufficient to achieve high strength. At the amplitude of 72 μm, a strength of 10 MPa or more can be achieved in approximately 0.6 seconds.

At the amplitude of 36 μm, it took approximately 2.5 s to reach 10 MPa or more, almost three times longer than at 72 μm. At the amplitude of 54 μm, the strength tends to increase with the welding time after 0.8 s. At the amplitude of 36 μm, the strength remains low until the welding duration of 2 s. However, with the extension of the welding time to 2.5 s, the shear strength notably increases, exceeding 15 MPa. Additionally, a slight decrease in strength is observed with the extension of the welding time to 3 s.

Analysis of the fracture surface shows that the extension of the welding time at the amplitude of 72 μm results in significant fiber flow from the fracture surface. At the same time, at the amplitude of 54 μm, the fiber flow is minimal even at extended welding times. This suggests that after the melting of the interface resin, the flow of resin and fibers is affected by amplitude. At the amplitude of 36 μm (Fig. 4), the resin partially disappeared in the weld after 2.5 s of welding. This phenomenon was attributed to the prolonged heating of a portion of the welding surface, leading to the thermal decomposition of the resin. To understand the reason for the differences in the fracture surfaces after welding, it is crucial to know the temperature history at the interface and in its vicinity.

3.2. Temperature Distribution Captured using the Thermographic Camera

Figures 5–7 present the temperature distribution on the side of the overlapping area, which was measured at each amplitude using a thermographic camera. Figure 5 shows that at the amplitude of 72 μm, the area near the interface is heated at 0.2 s, with a significant temperature increase at the right end of the interface.

Additionally, a rise in temperature was noted at the point of contact between the sonotrode and the upper adherend's left end. Sustained heat release was focused at the interface, 0.4 seconds after the experiment began, whereas the temperature increase at the upper adherend and the sonotrode contact point occurred later.

The high-temperature region spreads out after 0.6 s. This could be molten resin flowing out from the right of the interface. The zone near the interface is generally hotter than 150 °C. Additionally, at the 0.8 s mark, a temperature increase is observed at the contact point between the sonotrode and the upper adherend.

Although the exact mechanism causing this temperature increase is not yet understood, it is hypothesized that the observed heating is due to the friction between the sonotrode and the upper adherend. This heating may be caused by the decrease in adhesion as the upper adherend sinks downward.

Figure 6 shows the temperature distribution for the amplitude of 54 μm. Notably, the temperature increase is more gradual than at the amplitude of 72 μm. It is apparent that for the amplitude of 72 μm, at 0.4 s, the temperature is higher than that at 0.2 s post-oscillation.

Differences in the warping and surface roughness of each specimen are the likely reason for the variability in temperature increase across the interface in different experiments.

At 1.0 s after the vibration, the temperature of the entire interface is above 150 °C, and at the right end of the interface a spread of high-temperature region is observed, which could be an indication of resin outflow.

The temperature distribution for the amplitude of 36 μm is shown in Fig. 7. At this amplitude, the entire interface reached above 150 °C after almost 2.5 s of welding. During this time, the heat was transferred from the interface, and by the end of the welding process, a large amount of material around the weld was heated to above 80 °C.

The propagation of high-temperature regions from the interface can affect the cooling rate, which can, in turn, impact the resin flow near the interface, residual thermal stress, and degree of crystallinity. At the same time, the contact area of the sonotrode warms up toward the end of welding.

3.3. Temperature distribution in the thickness direction of the welded area

Figures 8–10 show the temperature distribution in the thickness direction of the welded section.

The horizontal axis represents the Y distance, measured from the center of the lap section at the sonotrode contact point to the considered point, as shown in Fig. 2. The vertical axis represents the temperature captured by the thermographic camera.

The temperature distribution is symmetrical and centered around the upper and lower adherents' interface, regardless of the amplitude. Additionally, the higher the amplitude, the faster the temperature rise. After

the interface temperature had risen to near the melting point of the matrix resin (polypropylene), which is around 160 °C, the temperature distribution changed from a one-peak to a two-peak pattern.

The reason for the change of the single-peak temperature distribution into two-peak one is believed to be that the resin at the interface entirely melted and flowed, and this flowing resin was measured. As shown in Fig. 10, at the amplitude of 36 μm, heat generated at the interface was transmitted, and a high-temperature region spread outward from the surface of the adherend.

Figure 11 shows the maximum temperatures in the temperature distributions in Figs. 8–10, plotted against time. During the initial phases of welding, the temperature increased uniformly across all amplitudes. However, as the temperature approaches 50 °C, the rate of temperature change begins to differ depending on the amplitude. Notably, the temperature increase at the interface is faster at higher amplitudes.

Furthermore, when the temperature of the interface reaches approximately 100 °C, the rate of temperature rise increases and is approximately the same for all amplitudes. Figure 12 shows the calculated full width at half maximum (FWHM) for the temperature distributions in Fig. 8–10. The maximum temperature is on the horizontal axis and FWHM on the vertical axis.

For amplitudes of 54 and 72 μm, the FWHM during welding is almost the same. For a smaller amplitude of 36 μm, the slope of FWHM is about twice steeper than those observed for other amplitudes. This suggests that a greater amount of material around the joint surface reaches higher temperatures even at the same interface temperature. It is thus suggested that differences in temperature over time may affect the extent of thermal decomposition due to the heating of the adherend in various regions.

4. Conclusion

We measured the temperature distribution during ultrasonic bonding of CF/PP using a thermographic camera and analyzed the obtained temperature distribution. The following results were obtained:

- By employing a welding fixture that allowed only the vertical movement of the upper substrate, we were able to measure a temperature distribution from the side that was nearly symmetrical above and below the interface.
- Temperature distribution in the overlapped side part during welding was used to effectively investigate the heating and bonding near the interface based on welding parameters.

- Evaluating the temperature distribution of the adherend from the side not only allows for the assessment of the interface but also enables the evaluation of heat generation at the sonotrode contact area.
- Lap joint tests were performed on specimens that underwent ultrasonic welding under varying conditions, followed by the observation of the fracture surface. The shape of the fracture surface significantly differed depending on welding conditions, even when the strength remained the same. The highest strength was attained by choosing welding conditions with minimal shape changes and reduced impact from thermal decomposition.
- By applying the half-width method to the measured temperature distribution in the thickness direction of the adherend, we assessed the spread of the high-temperature region centered on the welding interface. In this study, at a small amplitude (36 μm), the half-width of the maximum temperature showed approximately twice higher slope than at other amplitudes, indicating a wider high-temperature range even at the same interface temperature. The wide range of high temperatures may have affected both the welding strength and the degree of thermal decomposition.

Acknowledgements: This paper is based on results obtained from a project, JPNPP20004, subsidized by the New Energy and Industrial Technology Development Organization (NEDO).

References

1. Omairey SL., Sampethai S., Hans L, Worrall C, Lewis S, Negro D, Sattar T, Ferrera E, Blanco E, Wighton J, Muijs L, Veldman SL., Doldersum M, Tonnaer R, Jayasree N, & Kazilas M. Development of innovative automated solutions for the assembly of multifunctional thermoplastic composite fuselage. Int. J. Adv. Manuf. Technol. 2021; 117:1721–1738.
2. Ageorges C, Ye L, Hou M. Advances in fusion bonding techniques for joining thermoplastic matrix composites: a review. Compos A Appl 2001; 32(6):839-857.
3. Yousefpour A, Hojjati M, Immarigeon JP. Fusion bonding/welding of thermoplastic composites. J. Thermoplast. Compos. Mater. 2004; 17(4):303–341.
4. Bhudolia SK, Gohel G, Leong KF, Islam A. Advances in ultrasonicwelding of thermoplastic composites: A review. Materials, 2020 ;13(6): 1284; https://doi.org/10.3390/ma13061284.
5. Tutunjian S, Dannemann M, Fischer F, Eroğlu O, Modler N. A control method for the ultrasonic spot welding of fiber-reinforced thermoplastic laminates through the weld-power time derivative. J. Manuf. Mater. Process. 2019;3(1): 1; https://doi.org/10.3390/JMMP3010001.
6. Villegas IF. Strength development versus process data in ultrasonic welding of thermoplastic composites with flat energy directors and its application to the definition of optimum processing parameters. Compos Part A Appl Sci Manuf 2014;65:27–37.
7. Palardy G, Fernandez Villegas I. ULTRASONIC WELDING OF THERMOPLASTIC COMPOSITES WITH FLAT ENERGY DIRECTORS: INFLUENCE OF THE THICKNESS OF THE ENERGY DIRECTOR ON THE WELDING PROCESS. In: Proceedings of ICCM-20 Conference. Copenhagen, July, 2015. p.19-24.
8. Liu SJ, Chang IT. Factors Affecting the Joint Strength of Ultrasonically Welded Polypropylene Composites. Polym. Compos. 2001; 22(1):132-141.
9. Villegas IF, Palardy G. Ultrasonic welding of CF/PPS composites with integrated triangular energy directors: melting, flow and weld strength development. Compos Interfaces 2017;24:515–28.
10. Tao W, Su X, Wang H, Zhang Z, Li H, Chen J. Influence mechanism of welding time and energy director to the thermoplastic composite joints by ultrasonic welding. J Manuf Process 2019;37:196–202.
11. Jongbloed B, Teuwen J, Benedictus R, Villegas IF. On differences and similarities between static and continuous ultrasonic welding of thermoplastic composites. Compos B Eng 2020;203.
12. Qiu J, Zhang G, Sakai E, Liu W, Zang L. Thermal welding by the third phase between polymers: A review for ultrasonicweld technology developments. Polymers 2020;12(4), 759; https://doi.org/10.3390/polym12040759.
13. Levy, S. Le Corre, N. Chevaugeon, A. Poitou, A level set based approach for the finite element

simulation of a forming process involving multiphysics coupling: Ultrasonic welding of thermoplastic composites. Eur J Mech A Solids 2011;30(4), 501-509.

14. Tutunjian S, Dannemann M, Modler N, Kucher M, Fellermayer A. A numerical analysis of the temporal and spatial temperature development during the ultrasonic spot welding of fibre-reinforced thermoplastics. J. Manuf. Mater. Process. 2020, 4(2), 30; https://doi.org/10.3390/jmmp4020030.
15. Koyanagi J, Takamura M, Wakayama K, Uehara K, Takeda S. Numerical simulation of ultrasonic welding for CFRP using energy director. Advanced Composite Materials 2022;31(4):428–441.

Figure Captions

Fig. 1 Experimental setup for ultrasonic welding: (a) photograph, (b) schematic.

Fig. 2 Side view of the overlapping area of two adherends: (a) photograph, (b) schematic with the area observed using the thermography camera. Y is the direction of temperature distribution aligned with the sonotrode tip center line.

Fig. 3 Fracture surface under different welding times and sonotrode amplitudes: (a) 36 μm, (b) 54 μm, and (c) 72 μm.

Fig. 4 Overheated area of the fracture surface when welding at the amplitude of 36 μm for 2.5 s: (a) fracture surface and (b) enlarged view of the overheated area.

Fig. 5 Temperature distribution on the side of the overlapping area of the lap joint at the sonotrode amplitude of 72 μm, recorded using a thermographic camera.

Fig. 6 Temperature distribution on the side of the overlapping area of the lap joint at the sonotrode amplitude of 54 μm, recorded using a thermographic camera.

Fig. 6 Temperature distribution on the side of the overlapping area of the lap joint at the sonotrode amplitude of 54 μm, recorded using a thermographic camera.

Fig. 8 Temperature distribution in the thickness direction of the welded part at the amplitude of 72 μm and welding time of 0.8 s.

Fig. 9 Temperature distribution in the thickness direction of the welded part at the amplitude of 54 μm and welding time of 1.0 s.

Fig. 10 Temperature distribution in the thickness direction of the welded part at the amplitude of 36 μm and welding time of 2.5 s.

Fig. 11 Maximum temperature for each sonotrode amplitude in the temperature distribution in the thickness direction at the center of the welded layer.

Fig. 12 Full width at half maximum at each amplitude of the temperature distribution in the thickness direction at the center of the welded layer for each amplitude

Tables

Table 1 Lap shear strength under each welding condition.

Sonotrode amplitude [μm]	Welding time [s]	Strength [MPa]	
		Average	Standard deviation
36	2.0	6.5	3.3
	2.5	14.8	0.4
	3.0	14.7	1.2
54	0.8	12.3	3.1
	1.0	14.8	1.2
	1.4	17.4	1.2
72	0.6	14.0	2.0
	0.8	15.8	2.7
	1.0	15.4	0.3

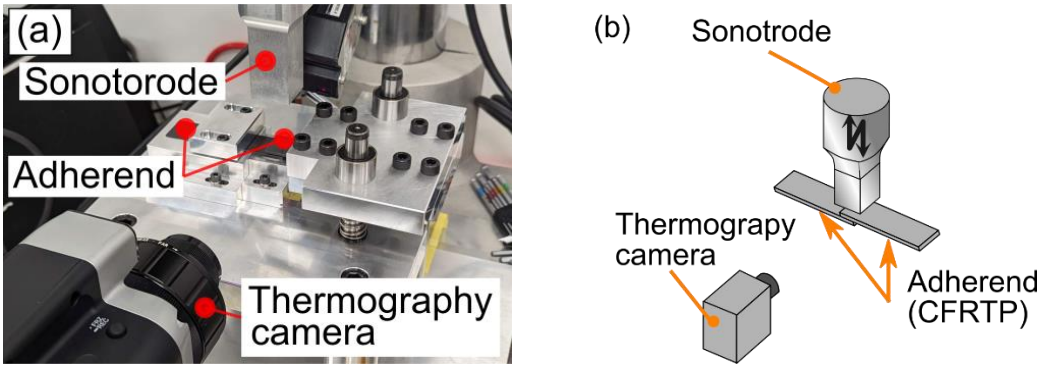

Fig. 1

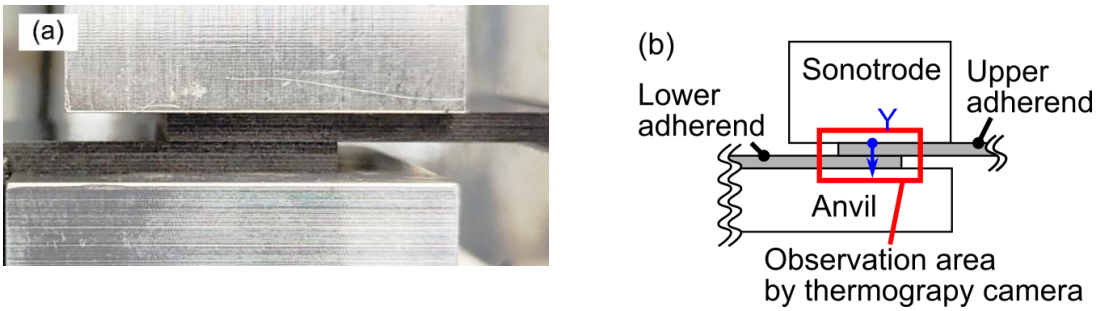
(a)
(b)
Sonotrode
Upper
adherend
Lower
adherend
Y
Anvil
Observation area
by thermograpy camera

Fig. 2

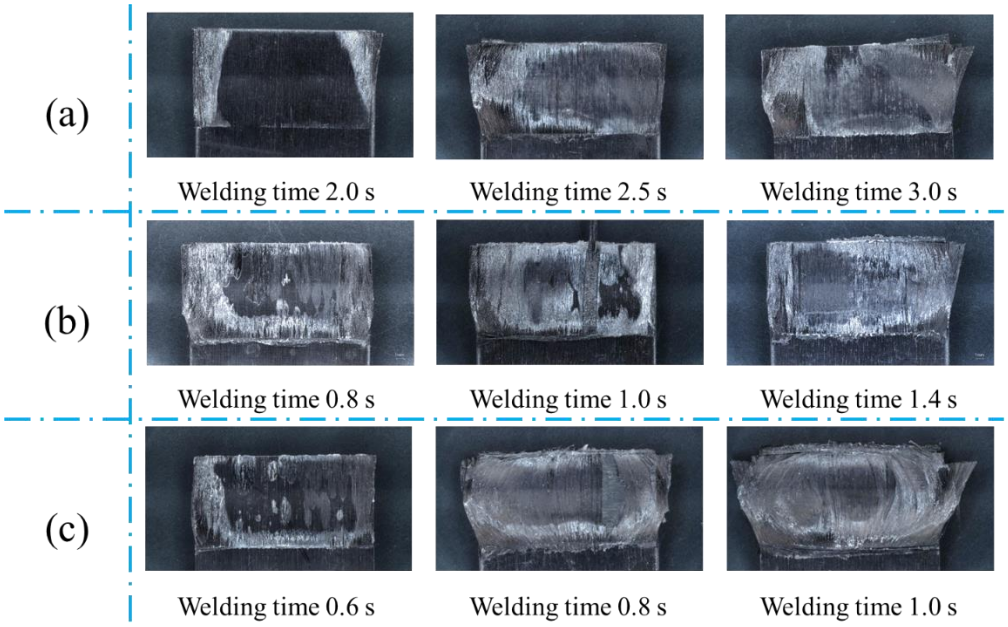
(a)
Welding time 2.0 s
Welding time 2.5 s
Welding time 3.0 s
(b)
Welding time 0.8 s
Welding time 1.0 s
Welding time 1.4 s
(c)
Welding time 0.6 s
Welding time 0.8 s
Welding time 1.0 s

Fig. 3

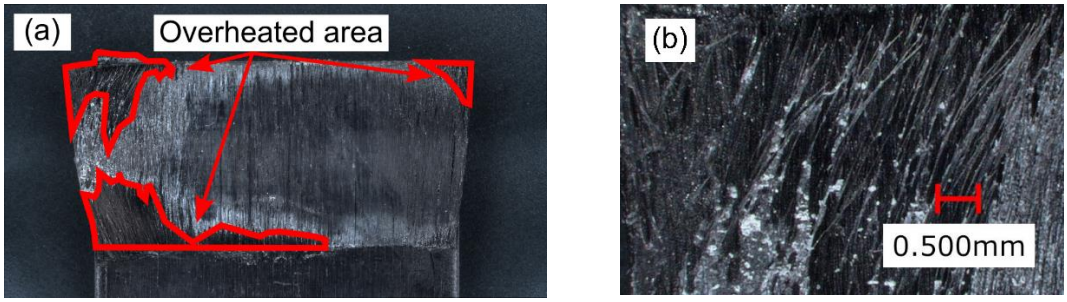

Fig. 4

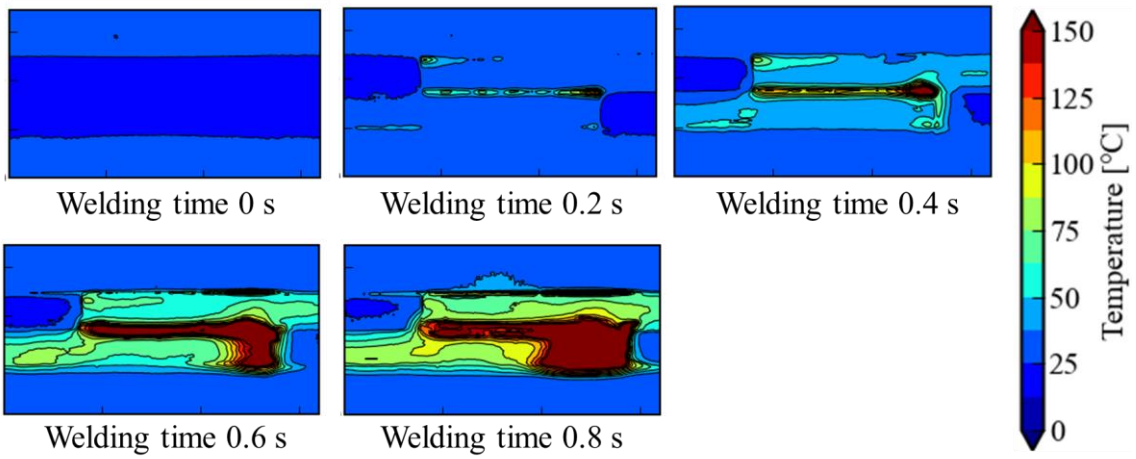
Welding time 0 s
Welding time 0.2 s
Welding time 0.4 s
Welding time 0.6 s
Welding time 0.8 s
150
125
100
75
50
25
0
Temperature [°C]

Fig. 5

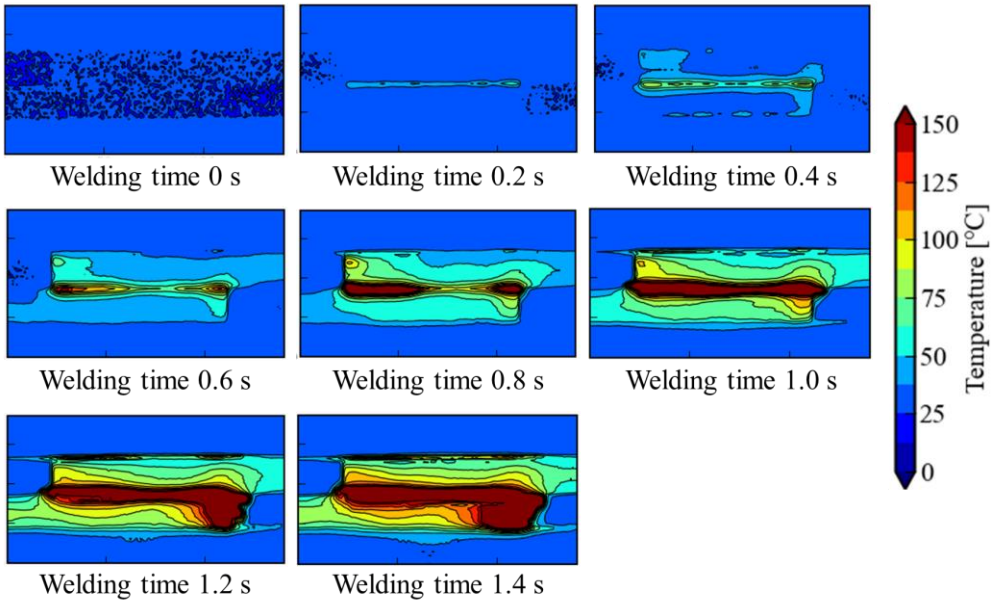
Welding time 0 s
Welding time 0.2 s
Welding time 0.4 s
Welding time 0.6 s
Welding time 0.8 s
Welding time 1.0 s
Welding time 1.2 s
Welding time 1.4 s
150
125
100
75
50
25
0
Temperature [°C]

Fig. 6

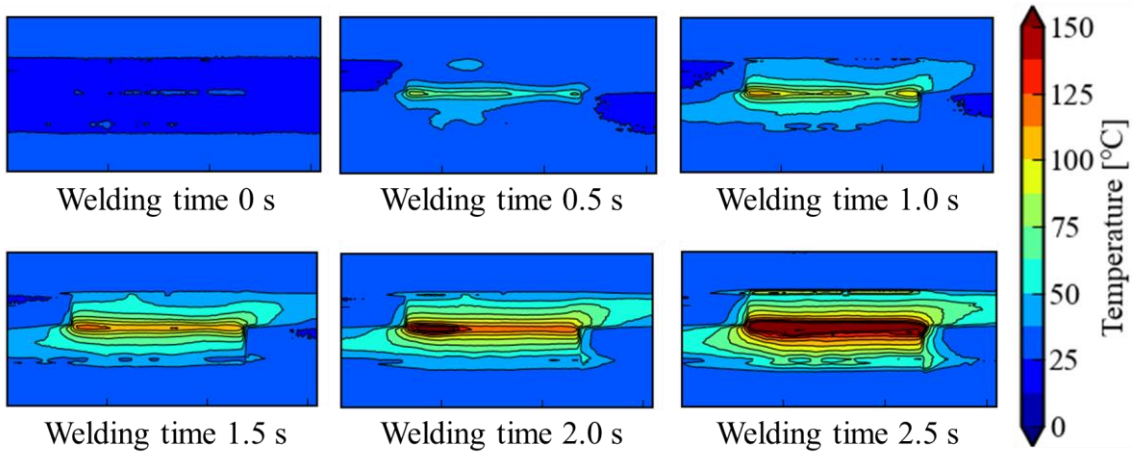
Welding time 0 s
Welding time 0.5 s
Welding time 1.0 s
Welding time 1.5 s
Welding time 2.0 s
Welding time 2.5 s
150
125
100
75
50
25
0
Temperature [°C]

Fig. 7

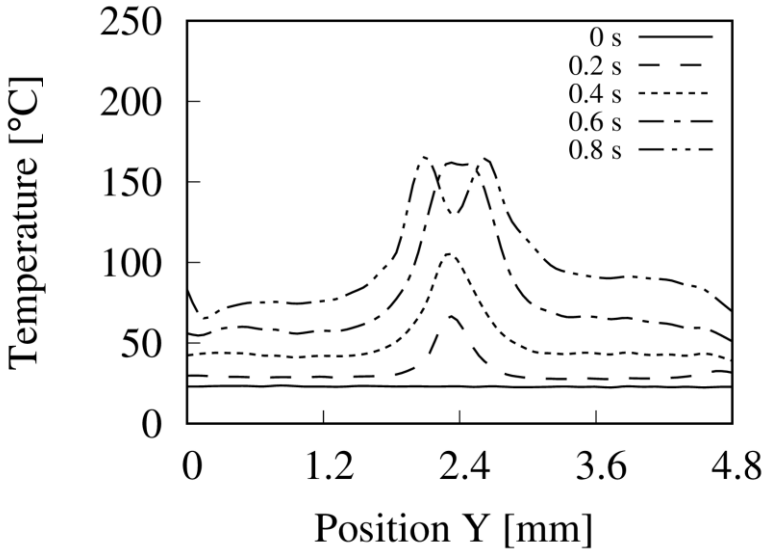
250
200
150
100
50
0
Temperature [°C]
0
1.2
2.4
3.6
4.8
Position Y [mm]
0 s
0.2 s
0.4 s
0.6 s
0.8 s

Fig. 8

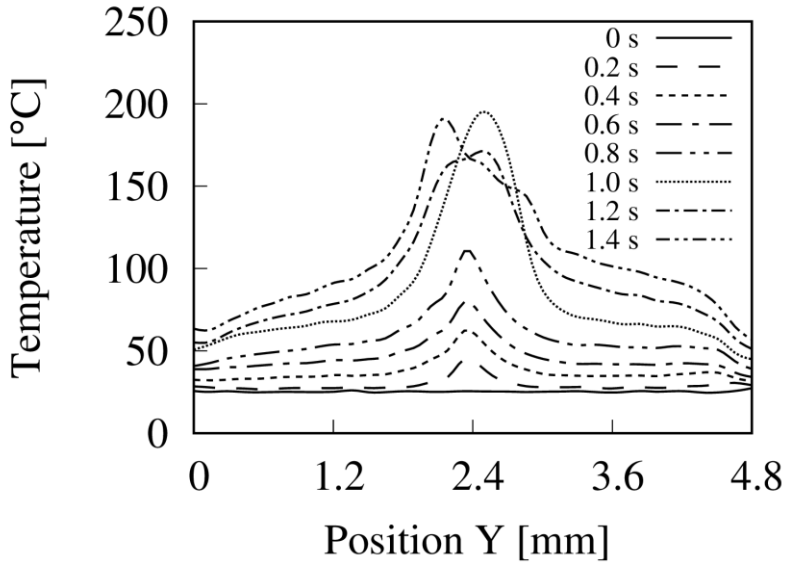
Temperature [°C]
250
200
150
100
50
0
0
1.2
2.4
3.6
4.8
Position Y [mm]
0 s
0.2 s
0.4 s
0.6 s
0.8 s
1.0 s
1.2 s
1.4 s

Fig. 9

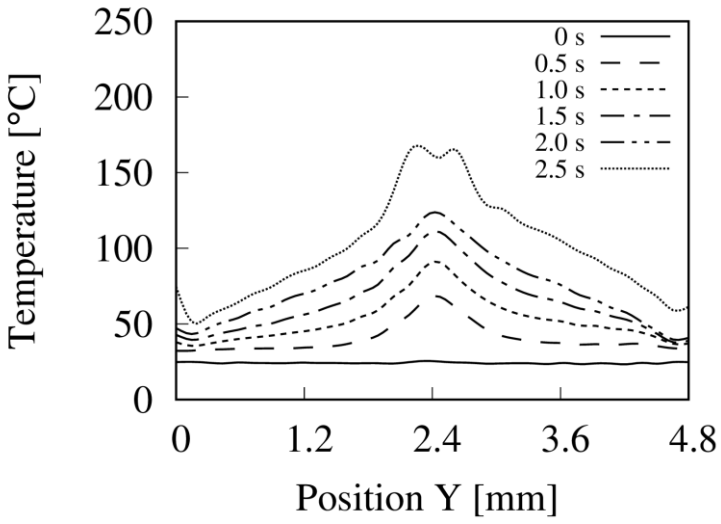
250
200
150
100
50
0
Temperature [°C]
0
1.2
2.4
3.6
4.8
Position Y [mm]
0 s
0.5 s
1.0 s
1.5 s
2.0 s
2.5 s

Fig. 10

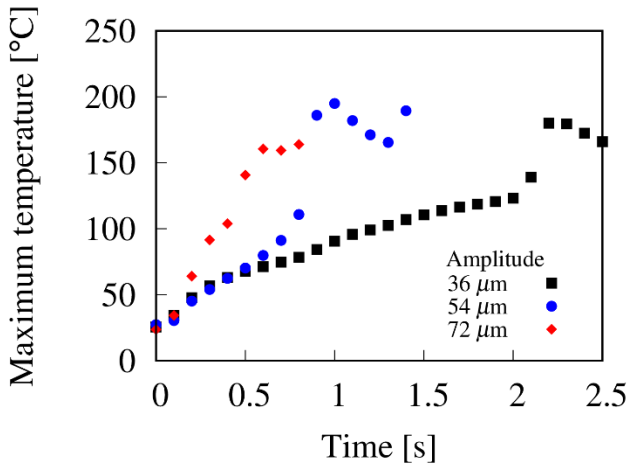
Maximum temperature [°C]
250
200
150
100
50
0
0
0.5
1
1.5
2
2.5
Time [s]
Amplitude
36 μm
54 μm
72 μm

Fig. 11

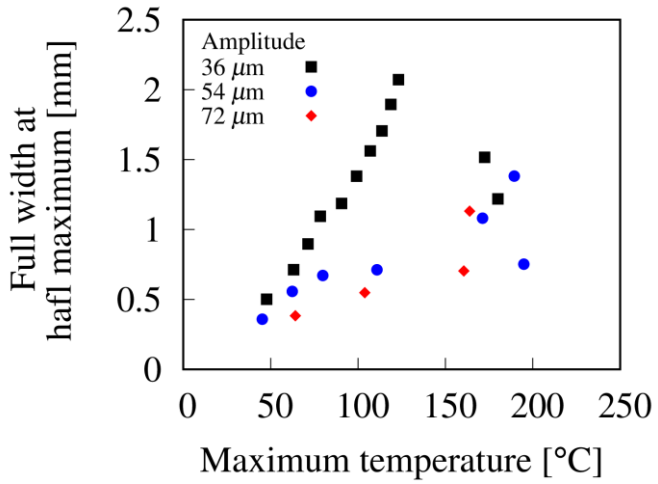
Full width at
hafl maximum [mm]
2.5
2
1.5
1
0.5
0
Amplitude
36 μm
54 μm
72 μm
0
50
100
150
200
250
Maximum temperature [°C]

Fig. 12